Macromolecular Reaction Engineering
www.mre-journal.de

Kinetic Investigation of the Emulsion Polymerization of Vinylidene Fluoride

*Burak Hanamirian, Azzurra Agostini, Isabelle Chaduc, Giulio Brinati, Bradley Kent, Giuseppe Storti, and Mattia Sponchioni**

This article is in memory of Prof. Mamoru Nomura, pioneer and master of emulsion polymerization. His first-rate scientific competence was no less than his humanity and kindness, which made him so appreciated by the entire Polymer Reaction Engineering community

Poly(vinylidene fluoride) (PVDF) is among the most produced fluoropolymers, second only to polytetrafluoroethylene. Despite its popularity, the complex microstructural properties achieved during the polymerization are not well documented in the literature. In particular, available models only track the chain length distribution of the polymer, while neglecting the distribution of other important properties, affecting the final behavior of the product. In this work, a 2D kinetic model, evaluating not only the chain length but also the number of terminal double bonds (TDBs) per chain, is developed. The numerical solution of the model is achieved by fractionating the population of polymer chains into classes with a specific number of TDBs and using the method of moments for each class. The model results are compared with experimental evidences for the amount of produced polymer, moles of main chain-ends, number, and weight average molecular weight as well as full molecular weight distribution. Based on this comparison, kinetic parameters are estimated by optimization using genetic algorithm. The model reliability is finally verified using additional experimental data at different temperatures and amounts of initiator.

1. Introduction

Fluorinated polymers, which are high-value, specialty polymers, find applications in many different areas due to their important and unique properties such as high resistance to aging and oxidation, thermal stability, and high hydrophobicity (due to their low surface tension), being inert to acids, bases, oils and solvents.[1–6] Fluorinated polymers cover a wide range of materials like thermoplastics, elastomers, semi-crystalline and amorphous materials. Due to these properties, they are used in many industrial sectors including construction, industrial coating and painting, aerospace, automotive, petrochemistry, and photonics.[1,3,4,7]

Poly(vinylidene fluoride) (PVDF) reached the second largest volume, following polytetrafluoroethylene, among fluoropolymers due to its processability and excellent combination of properties.[1,4,8] Industrially, PVDF is mostly produced by suspension and emulsion polymerization.[1,9] A wide literature is available to interested readers providing the mechanistic picture of such heterogeneous polymerization processes.[10–16] Homopolymers of vinylidene fluoride (VDF) are long-chain macromolecules with semi-crystalline form, and contain 3.2 wt% hydrogen, and 59.4 wt% fluorine atoms. Even though PVDF is used in various high-tech applications, there are also some disadvantages: for example, high melting temperatures cause processing costs to be large, it is hardly soluble in common organic solvents and it is complicated to be cured.[1]

In order to overcome these limitations, a good knowledge of its microstructure is important to understand the behavior of PVDF based on the specific applications. Unfortunately, due to the complexity of the reactions taking place in the high-pressure, semi-batch reactors working with gaseous VDF, and to the multi-phase nature of the reacting system, accurate models for the detailed description of the polymer microstructure are missing in the literature.[17] Therefore, a comprehensive kinetic scheme including all the reactions involved in the VDF

B. Hanamirian, G. Storti, M. Sponchioni
Department of Chemistry
Materials and Chemical Engineering "Giulio Natta"
Politecnico di Milano
Via Mancinelli 7, Milano 20131, Italy
E-mail: mattia.sponchioni@polimi.it
A. Agostini, I. Chaduc, G. Brinati
Syensqo S.A. – Solvay Specialty Polymers Italy S.p.A
Viale Lombardia 20, Bollate 20021, Italy
B. Kent
Syensqo S.A. – Solvay Solexis Inc.
10 Leonard Lane, West Deptford, NJ 08086, USA

The ORCID identification number(s) for the author(s) of this article can be found under https://doi.org/10.1002/mren.202400023

DOI: 10.1002/mren.202400023

polymerization process and especially an accurate estimation of the corresponding rate constants is urgently required.[18]

The main aim of this work is the development of a kinetic model accounting for the main reactions involved in the production of PVDF by emulsion polymerization and able to predict the detailed microstructure of the product. Namely, the molecular weight distribution as well as the distribution of the terminal double bonds are calculated along with average values of other chain end groups and long branches. As a result, each polymer chain is characterized by two parameters, which are the number of repeating units and terminal double bonds (TDBs), the latter being responsible for chain branching. This further expands the understanding of the heterogeneity of the polymer obtained during the emulsion polymerization and the main factors contributing to it. For the selected reaction pathways, the evaluation of the involved kinetic constants is carried out comparing the model predictions with experimental data of a reference reaction for the amount of produced polymer, chain-ends and molecular weight distributions. Moreover, the model reliability is confirmed by comparing its predictions for additional experiments at different temperature and initiator concentration. With this 2D model, the accurate prediction of multimodal molecular weight distributions, typically associated to the branching reactions taking place during these processes, is feasible.

2. Model Development

With reference to the emulsion polymerization of VDF in a semi-batch reactor, the following main assumptions have been considered for model development:[18]

1) Negligible mass-transport limitations: during the polymerization, the interphase partitioning of the monomer and chain transfer agent (CTA) is assumed to be at equilibrium.
2) For the radical species, quasi-steady-state assumption (QSSA) is considered.
3) Due to the large molecular weights involved, the dependence of the chain composition on chain length is neglected (long-chain assumption, LCA).
4) Given the different nature of the radicals in the system (determined by the arrangement of the last monomer unit in the chain) the nature of the terminal unit of active chains is accounted for and it is assumed that only such unit determines chain reactivity.
5) Negligible water solubility for the monomer.[1,19,20]
6) Pseudo-bulk system: the rate of polymerization is assumed independent of the particle size and number. This means the system is non-compartmentalized, and the polymerization can be described as a bulk process due to the large number of radicals per particle. Accordingly, the particle size distribution is not accounted for in the model. This key assumption will be validated in Section 3.1.

2.1. Kinetic Scheme

The main reactions expected to take place in the studied system are reported in **Table 1** with the notation used in the model. For clarity, the chemical structure of all species mentioned in the table is explicitly reported in Table S1 (Supporting Information).

Table 1. Kinetic Scheme of VDF Polymerization.

Initiation	$I_2 \xrightarrow{k_d} 2I^\bullet$
	$I^\bullet \xrightarrow{k_{int}} T + S^\bullet$
Propagation	$S^\bullet + M \xrightarrow{k_{pM}} R_1^\bullet$
	$T^\bullet + M \xrightarrow{k_{pM}} R_1^\bullet$
	$R_n^\bullet + M \xrightarrow{k_{pM}} R_{n+1}^\bullet$
Chain Transfer to Monomer	$R_n^\bullet + M \xrightarrow{k_{fM}} R_1^\bullet + P_n^=$
	$R_n^\bullet + M \xrightarrow{k_{fM2}} R_1^{\bullet=} + P_n$
Propagation to Terminal Double Bond (TDB)	$R_n^\bullet + P_m^= \xrightarrow{k_{TDB}} R_{n+m}^\bullet$
Chain Transfer to CTA	$R_n^\bullet + T \xrightarrow{k_{fT}} P_n + T^\bullet$
Chain Transfer to Polymer	$R_n^\bullet + P_m \xrightarrow{k_{fP}} R_m^\bullet + P_n$
Back-Biting	$R_{n,CF2}^\bullet \xrightarrow{k_{bb1}} R_{n,MC}^\bullet$
	$R_{n,CH2}^\bullet \xrightarrow{k_{bb2}} R_{n,MC}^\bullet$
Bimolecular Termination (Disproportionation)	$R_n^\bullet + R_m^\bullet \xrightarrow{k_{td}} P_n^= + P_m$

As shown in Table 1, the thermal initiator (di-tert-butyl peroxide, DTBP, indicated in the scheme as I_2), is decomposed into two tert-butoxy (TBO, $I^\bullet$) radical fragments. This species further decomposes into acetone which acts as a chain-transfer agent (CTA, T) and a different radical fragment ($CH_3^\bullet$, $S^\bullet$) which is actually starting the active chains.[9,21]

Three different propagation reactions take place in the system, where VDF reacts with either a radical fragment $S^\bullet$ produced by initiation, the radical from the CTA ($T^\bullet$) or with a growing active chain with any length ($R_n^\bullet$), thus producing a chain with one more monomer unit.

Chain transfer to monomer reactions occur between an active chain of any length and VDF. We differentiated among two different reactions. In one case, a hydrogen from the active chain is abstracted and attached to the monomer, causing it to become a monomeric radical ($R_1^\bullet$), while a dead polymer chain containing a TDB is formed ($P_n^=$). The second case occurs when a monomer loses one hydrogen atom forming a radical ($R_1^{\bullet=}$). This is considered as a TDB in the model since it will remain at one end as the polymer grows. On the other hand, the active chain which captured the hydrogen terminates to dead polymer (P_n).

The TDB mentioned in the previous paragraph can also be formed by bimolecular termination (disproportionation). In this case, two active chains get into contact and one hydrogen is transferred from one to the other forming two chains of dead polymer, out of which only one (the one that lost the hydrogen) contains a TDB.

Notably, such TDB can react like any other double bond in the system by propagation: this reaction consumes TDB (propagation to TDB) and takes place when a dead polymer with a TDB reacts with an active chain forming a mid-chain radical. It should be noted that this reaction is the only one combining two chains in the considered kinetic scheme, and hence has a potential of causing a step growth of the chain if two chains with similar length undergo this type of reaction.

The chain transfer to CTA takes place between an active chain of any length and the CTA, where one hydrogen atom from the CTA is abstracted by the active chain producing a dead polymer as well as a radical fragment from CTA.

In the chain transfer to polymer, a dead chain P_m reacts with an active chain $R_n^{\bullet}$ resulting in the abstraction of hydrogen and the formation of the same type of species with reversed lengths ($R_m^{\bullet}$ and P_n, respectively).

Back-biting reactions do not cause a change in the length of the chains but cause a radical located at the end of the chain to move to a backward position along the chain, thus forming a mid-chain radical ($R_{n,MC}^{\bullet}$) and a very short branch, whose impact on the polymer behavior can be considered negligible.

Unlike some of the previous works,[1,9] which assumed bimolecular termination reactions occur only by recombination, bimolecular termination is assumed to happen only by disproportionation just like experimentally proven by Apostolo et al.[18] Namely, the average number of chain-ends coming from initiation was measured slightly larger than one, while two chain-ends of this type are expected when recombination is the dominant termination reaction. Note that a value slightly larger than one is fully reasonable because other reactions, such as propagation to TDB, combine chains, thus resulting in chains with more than one initiation-type chain-end.

An additional complication is related to the different arrangement of the monomer units along the polymer chain. As a matter of fact, two different chain-ends for the active chains are possible: "tail type", where the chain ends with $CH_2^{\bullet}$ and "head type" where the chain ends with $CF_2^{\bullet}$.[1,4,8,18] Therefore, four possible propagation reactions were considered:

Head to head addition $RCH_2CF_2^{\bullet} + CH_2CF_2 \xrightarrow{k_{HH}} RCH_2CF_2CH_2CF_2^{\bullet}$ (1)

Head to tail addition $RCH_2CF_2^{\bullet} + CH_2CF_2 \xrightarrow{k_{HT}} RCH_2CF_2CF_2CH_2^{\bullet}$ (2)

Tail to head addition $RCF_2CH_2^{\bullet} + CH_2CF_2 \xrightarrow{k_{TH}} RCF_2CH_2CH_2CF_2^{\bullet}$ (3)

Tail to tail addition $RCF_2CH_2^{\bullet} + CH_2CF_2 \xrightarrow{k_{TT}} RCF_2CH_2CF_2CH_2^{\bullet}$ (4)

As indicated by previous experimental works[18] and by quantum chemical simulations,[22] the addition reactions occur in large favor of producing $CF_2^{\bullet}$ (head type) radicals rather than the tail type. Accordingly (further discussed in Section 3.1), it can be seen that the rate constants for the reactions producing head type radicals (k_{HH} and k_{TH}) are much larger than those producing tail type ones (k_{HT} and k_{TT}). Once the values of the rate constants are available, the fraction of radicals of head or tail type can be estimated from the corresponding rate constants by the following equations (5) and (6):

$$\phi_H = \frac{k_{TH}}{(k_{TH} + k_{HT})} \tag{5}$$

$$\phi_T = 1 - \phi_H \tag{6}$$

Note that, in agreement with this approach, all the rate constants of the reactions in Table 1 are actually "composition-average rate constants", which take both head and tail type radicals into account, with the exception of the back-biting reactions only. In fact, these reactions play a major role in the production of CF_2H and CH_3 chain-ends, in case a head or tail type radical is involved, respectively: therefore, to properly track the formation of such end groups, the two reactions have been differentiated in this case.

2.2. Material Balances

The gaseous monomer (VDF), represented by M, is continuously fed to the reactor in order to keep the reaction pressure constant. Its equilibrium concentration in the polymer phase is described by the Henry-type relation in Equation (7), where H is the Henry constant for the monomer in polymer and P is the absolute pressure. The overall rate of polymerization, R_p ($mol\ min^{-1}$), is obtained by Equation (8), which is calculated by multiplying the propagation rate constant, k_{pM}, with the concentration of monomer, M, and the total moles of active chains, Λ_0. Finally, the differential equation used to predict the volume of produced polymer, V_p, is reported in Equation (9), where $M_{wt,\ mon}$ represents the molecular weight of monomer, and ρ_P and ρ_M represent the density of polymer and monomer, respectively.

$$M = HP \tag{7}$$

$$R_p = k_{pM}\, M\Lambda_0 \tag{8}$$

$$\frac{d\,V_p}{d\,t} = \frac{M_{wt,\ mon}}{\rho_P\left(1 - \frac{M\ M_{wt,\ mon}}{\rho_M}\right)} R_p \tag{9}$$

2.3. Method of Classes and Moment Equations

Different approaches can be used to derive the population balance equations for the active and dead polymer chains.[18,23] A 1D model, tracking only the chain length, could be one of the simplest ways to represent the system and the corresponding computational cost could be very low. However, a 1D model would fail to provide a detailed description of the system, in particular when highly-branched material is present, as in our case.

In this work, a 2D approach, referred to as "method of classes",[23] is used. With this approach, the total polymer population is divided into different "classes", each one defined by a specific chain property. Since the number of TDBs per chain is a crucial property for the developed model, to reliably track chain-ends and molecular weight distribution, each class has been defined based on the number of TDBs per chain. In other words, class 0 would have chains with no TDBs, class 1 would contain chains with 1 TDB only and so on. The population balance equations are derived so that the chain length and the number of TDBs per chain are tracked for polymer chain and those equations are reported in the Supporting Information (Equations S1 and S2, Supporting Information).

The numerical solution of the resulting population balances has been carried out by the method of moments.[24] In particular,

moments are defined with respect to the chain length for each single class, that is for each value of TDBs per chain:

$$\lambda_j\ (t) = \sum_{n=0}^{\infty} n^j R_{n,t} \tag{10}$$

$$\mu_j\ (t) = \sum_{n=0}^{\infty} n^j P_{n,t} \tag{11}$$

where $\lambda_j(t)$ and $\mu_j(t)$ are the moments of order j for active and dead chains, respectively, containing t TDBs per chain, while n is the number of repeating units. The moments of each class are expected to be especially effective to reconstruct the corresponding chain length distribution given the homogeneity achieved by fractionating the chain population in families characterized by the same number of TDBs per chain. The moment equations for the active chains and dead polymer are shown by Equations (12) and (13).

$$\begin{aligned}\frac{d\,\lambda_j\,(t)}{d\,t} &= \left(2fk_dI_2 + k_{fM}M\sum_{r=0}^{\infty}\lambda_0\,(r) + \frac{k_{fT}}{V_p}T\sum_{r=0}^{\infty}\lambda_0\,(r)\right)\delta_{t=0} \\ &+ \left(k_{fM2}M\sum_{r=0}^{\infty}\lambda_0\,(r)\right)\delta_{t=1} + k_{pM}M\sum_{h=0}^{j}\binom{j}{h}\lambda_h\,(t) \\ &- k_{pM}M\lambda_j\,(t) - k_{fM}M\lambda_j\,(t) - k_{fM2}M\lambda_j\,(t) \\ &- \frac{k_{TDB}}{V_p}\lambda_j\,(t)\sum_{r=0}^{\infty}r\mu_0\,(r) + \frac{k_{TDB}}{V_p}\sum_{h=0}^{j}\binom{j}{h}\sum_{r=0}^{t}(r+1)\,\lambda_{j-h} \\ &\times(t-r)\,\mu_h\,(r+1) - \frac{k_{fT}}{V_p}T\lambda_j\,(t) - \frac{k_{fP}}{V_p}\lambda_j\,(t)\sum_{r=0}^{\infty}\mu_1\,(r) \\ &+ \frac{k_{fP}}{V_p}\mu_{j+1}\,(t)\sum_{r=0}^{\infty}\lambda_0\,(r) - \frac{k_{td}}{V_p}\lambda_j\,(t)\sum_{r=0}^{\infty}\lambda_0\,(r)\end{aligned} \tag{12}$$

$$\begin{aligned}\frac{d\,\mu_j\,(t)}{d\,t} &= k_{fM}\,M\lambda_j\,(t-1) + k_{fM2}M\lambda_j\,(t) - \frac{k_{TDB}}{V_p}t\mu_j\,(t)\sum_{r=0}^{\infty}\lambda_0\,(r) \\ &+ \frac{k_{fT}}{V_p}T\lambda_j\,(t) + \frac{k_{fP}}{V_p}\lambda_j\,(t)\sum_{r=0}^{\infty}\mu_1\,(r) - \frac{k_{fP}}{V_p}\mu_{j+1}\,(t)\sum_{r=0}^{\infty}\lambda_0\,(r) \\ &+ \frac{1}{2}\frac{k_{td}}{V_p}\lambda_j\,(t-1)\sum_{r=0}^{\infty}\lambda_0\,(r) + \frac{1}{2}\frac{k_{td}}{V_p}\lambda_j\,(t)\sum_{r=0}^{\infty}\lambda_0\,(r)\end{aligned} \tag{13}$$

In these equations, n represents the chain length, j the order of moment, R is used for active chains and P for dead polymer, and the number of TDBs is shown by the letter t. δ is used for the Kronecker Delta Function, which is equal to 1 for the specified value and 0 for any other case. As typical for well-behaved chain length distributions,[24–29] the moments of the first three orders (zero-th, first and second orders) have been calculated for both the active chains, λ, and the dead polymer, μ. When higher order moments are involved (typically the third order moment of the dead polymer in the chain transfer to polymer reaction), the closure formula reported by Equation (14) is used.[30]

$$\mu_3\ (t) = 2\frac{\left(\mu_2\,(t)\right)^2}{\mu_1\,(t)} - \frac{\mu_2\,(t)\,\mu_1\,(t)}{\mu_0\,(t)} \tag{14}$$

If reconstruction of the molecular weight distribution (MWD) is of interest, it is achieved using again the approach from Hulburt and Katz.[30] Limiting the formula to the first three terms, the distribution as a function of chain length, n, and number of TDBs, t, could be obtained by Equation (15):

$$f\ (n,t) = \frac{b\,(t)\,/a\,(t)}{(b\,(t)-1)!}\,z(t)^{b(t)-1}\exp\left(-z\,(t)\right)\mu_0\,(t) \tag{15}$$

where, $a(t) = \frac{\mu_1(t)}{\mu_0(t)}$, $b(t) = \frac{\mu_1^2(t)}{\mu_2(t)\mu_0(t)-\mu_1^2(t)}$ and $z(t) = \frac{b(t)n}{a(t)}$.

2.4. Chain-Ends and Branches

In order to track chain-ends and branches formed in the polymer, dedicated material balances were introduced. In particular, due to the head-tail nature of the monomer, two different chain-ends (CF_2H and CH_3) can be formed depending on the specific arrangement of the monomer unit at the end of the growing chain, as shown in Equations (16) and (17).

$$\frac{d\,CF_2H}{d\,t} = \frac{k_{fP}}{V_p}\,\mu_1\Lambda_0\phi_H + k_{bb1}\Lambda_0 p_{HT}\phi_H + \frac{1}{2}\frac{k_{td}}{V_p}\Lambda_0^2\phi_H + \frac{k_{fT}}{V_p}T\Lambda_0\phi_H \tag{16}$$

$$\begin{aligned}\frac{d\,CH_3}{d\,t} &= \frac{k_{fP}}{V_p}\,\mu_1\Lambda_0\phi_T + k_{bb2}\Lambda_0 p_{HT}\phi_T + \frac{1}{2}\frac{k_{td}}{V_p}\Lambda_0^2\phi_T + \frac{k_{fT}}{V_p}T\Lambda_0\phi_T \\ &+ k_{pM}MS^{\bullet} + k_{pM}MT^{\bullet}\end{aligned} \tag{17}$$

Both chain-ends are formed by chain transfer to polymer, backbiting, termination and chain transfer to CTA. In addition, the CH_3 type chain-ends are also formed by propagation from the initiator fragment $S^{\bullet}$. In these equations, Λ_0 represents the sum of $\lambda_0(t)$ of all the classes, and similarly μ_1 represents the sum of $\mu_1(t)$ of all the classes. The terms are multiplied by the probabilities of having head and tail type radicals, which were already defined in Section 2.1. The probabilities of having a specific sequence of terminal monomer units (whose knowledge is useful to evaluate the back-biting reactions) have been defined as in Equations (18–21). For example, p_{TH} is the probability of having a head type radical from a chain which was tail type.

$$p_{TH} = \frac{k_{TH}}{\left(k_{TH}+k_{TT}\right)} \tag{18}$$

$$p_{TT} = \frac{k_{TT}}{\left(k_{TH}+k_{TT}\right)} \tag{19}$$

$$p_{HH} = \frac{k_{HH}}{\left(k_{HH}+k_{HT}\right)} \tag{20}$$

$$p_{HT} = \frac{k_{HT}}{(k_{HH} + k_{HT})} \tag{21}$$

The developed model does not track the distribution of branching points as a function of the chain length; however, an average value can be easily estimated. Since the number of TDBs per chain is closely related to the number of branches per chain (number of TDBs must not be greater than two more of number of branches), such average value can be compared with the average number of TDBs per chain to provide better understanding of the (average) chain microstructure. Such average values can be obtained using Equations (22) and (23).

$$\frac{d\,BP}{d\,t} = \frac{k_{fP}}{V_p}\,\mu_1\Lambda_0 + \frac{k_{TDB}}{V_p}\Lambda_0 \sum_{t=0}^{\infty} t\mu_0\,(t) \tag{22}$$

$$\frac{d\,TDB}{d\,t} = k_{fM}\,M\Lambda_0 + k_{fM2}M\Lambda_0 - \frac{k_{TDB}}{V_p}\Lambda_0 \sum_{t=0}^{\infty} t\mu_0\,(t) + \frac{1}{2}\frac{k_{td}}{V_p}\Lambda_0^2 \tag{23}$$

According to the kinetic scheme (Table 1), only chain transfer to polymer and the propagation to TDB lead to the formation of long branches and, as such, are considered in the formation of branching points. Even though the back-biting reactions are producing mid-chain radicals, they are not considered in the balance of the branching points since they will produce very short chain branches only. On the other hand, the balance for TDBs contains four terms: both of the chain transfer to monomer reactions, termination by disproportionation and propagation to TDB, the first three forming and the last one consuming TDBs.

2.5. Numerical Solution

To summarize, the developed model is made of $6N_c$+11 ordinary differential equations, where N_c represents the number of classes. The numerical solution of this system has been performed using the integrator ode15s in MATLAB. The estimation of missing parameter values was carried out using genetic algorithm, with a maximum number of generations of 100 and a population size of 200. To make sure the best agreement is achieved, a nonlinear optimizer (fmincon function of MATLAB) is used as a hybrid function. The optimization is allowed to change the parameters inside a given upper and lower bound limit, which is selected according to the parameters taken from the literature for similar systems. Initially, all the parameters were allowed to be optimized within an order of magnitude; in case the agreement was not good enough, the constraint of upper and lower limits were expanded to two orders of magnitude only for some specific parameters which are believed to play crucial role for having a good prediction. All the experimental data available are used in order to have the best possible estimation, and the fitness function is selected to use relative errors (Equation (24)). It is worth mentioning that the calculated error reaches very high values for the experimental data close to 0, this is due to the presence of the experimental values in the denominator of the equation. When this happens (for the two ends of the molecular weight distributions), the values causing large errors are neglected in order to have better results for the optimization.

$$\epsilon_{relative} = \sum \left(\frac{y_{exp} - y_{model}}{y_{exp}} \right)^2 \tag{24}$$

3. Results and Discussion

As anticipated, the method of classes was used to fractionate the population of polymer chains and apply the method of moments to each set of chains with specific number of TDBs. To implement this approach, the first step is to determine how many classes are needed for accurate model predictions. In theory, the number of classes N_c has to be infinite, as it is for the possible number of TBDs that a chain could present. However, simulations at increasing values of N_c clearly showed that the amount of polymer in the last classes is decreasing: this is logical due to the finite value of the maximum chain length when crosslinked polymer cannot be formed. Therefore, all the simulations were run using $N_c = 50$, where the amount of produced polymer in the last class is always smaller than a threshold value (typically ≈ 0.1% w/w, with respect to the total polymer produced).

Another important aspect on the experimental gel permation chromatography (GPC) data has to be mentioned. From independent runs, it is found that a fraction of polymer is insoluble in the solvent used for GPC in all samples, whose value lies in the range 5–10% of the total polymer. Such values are randomly distributed and show no visible trend with respect to the amount of produced polymer. Accordingly, a constant, average value of 8% of the polymer is assumed to be insoluble in the solvent and all the comparisons with the experimental GPC data have been performed properly considering this loss of sample mass. We assumed that classes containing highly-branched material are responsible for the insoluble polymer fraction. Therefore, after the simulation is completed, the amount of polymer corresponding to 8% w/w of the produced one is "separated" as insoluble part starting from the highest order classes. The molecular weight distribution (MWD) was then obtained by summing the MWDs of each class until the end of the soluble polymer. At the selected experimental conditions, the soluble polymer fraction is made of the first 15 classes (92% of the total polymer) only and the rest is the insoluble part. Therefore, all the comparisons between model and experimental number- and weight-average molecular weights as well as MWDs have been performed considering the classes representing the soluble polymer only. On the other hand, we did not observe insoluble polymer in the solvent used for nuclear magnetic resonance (NMR) analysis (i.e., deuterated acetone), hence the comparison of chain-ends and branches accounts for the whole mass of polymer sample. We consider this an evidence that gelation does not take place in our system, which is predicted by the model as well (divergence of the estimated moments for branched polymer is never observed).

Table 2. Modified Arrhenius Law Parameters for the Different Possible Propagation Reactions[22] and Values of the Rate Constants at the Upper and Lower Temperature Extremes of the Range used in.[18]

Rate Constant [$L\ mol^{-1}\ min^{-1}$]	k_0 [$L\ mol^{-1}\ min^{-1}$]	α	E_a/R [K]	k at 40 °C [$L\ mol^{-1}\ min^{-1}$]	k at 90 °C [$L\ mol^{-1}\ min^{-1}$]
k_{HH}	1.99×10^8	2.14	2468	8.31×10^4	3.38×10^5
k_{HT}	5.22×10^7	2.09	2189	5.32×10^4	1.90×10^5
k_{TH}	9.96×10^7	1.48	1567	7.16×10^5	1.78×10^6
k_{TT}	2.44×10^7	1.43	3197	9.62×10^2	4.85×10^3

Table 3. Literature Parameter Values and Corresponding Source.

Parameter	Value or Equation	Unit
k_d [31]	$1.94 \times 10^{17} \exp(-\frac{18621}{T\ [K]})$	min^{-1}
k_{int} [32]	$9.54 \times 10^{23}\ (T\ [K])^{-2.55} \exp(-\frac{8475}{T\ [K]})$	min^{-1}
H [18]	3.1×10^{-2}	$mol\ L^{-1}\ atm^{-1}$

3.1. Parameter Estimation

According to the quantum chemical simulations of Mavroudakis et al.[22] for the four different propagation reactions according to the last unit of the growing chain and the way the monomer is incorporated (mentioned in Section 2.1), the modified Arrhenius law parameters appearing in Equation (25) are reported in **Table 2**.

$$k = k_0 \left(\frac{T\ [K]}{298}\right)^{\alpha} \exp\left(-\frac{E_a}{RT}\right) \tag{25}$$

From the values of the rate constants at the upper and lower temperature extremes of the range used in the prior work (40–90 °C),[18] the reactions forming head type radicals (k_{HH} and k_{TH}) occur much faster than those forming tail type ones (k_{HT} and k_{TT}).

The values of the kinetic parameters at the reaction temperature used in this work are calculated accordingly and, using Equation (5), the probability of having head-type radicals is found to be larger than 85%, which suggests most of the active chains end with $CF_2^{\bullet}$ radical. It is worth mentioning that these different values of propagation rate constants are used for estimating the probabilities and hence the different end groups formed during the reaction. On the other hand, the model considers a single value for the propagation rate constant, which is calculated by parameter optimization as discussed later on. Even though there are no restrictions to the values of the different parameters, the estimated propagation rate constant is very close to the k_{HH} and k_{HT} values reported by Mavroudakis et al., thus confirming that head type radicals are much more probable than tail type ones.

The model developed in this work was calibrated in terms of rate constants by fitting the experimental results of conversion and concentration of specific end-groups during time using a genetic algorithm. The parameter values taken from the literature and used without any modifications are reported in **Table 3**. These include the initiator dissociation rate constant k_d, the rate constant for the decomposition of the initiator fragment k_{int} and the VDF Henry constant describing its solubility in the corresponding homopolymer.

Table 4. Parameters Optimized in This Work for Fitting of the Experimental Results.

Parameter	k_0 [$L\ mol^{-1}\ min^{-1}$ or min^{-1}]	E_a/R [K]
k_{pM}	6.05×10^{10}	4539[4]
k_{TDB}	6.51×10^8	4539
k_{fP}	1.58×10^6	4539[4]
k_{fM}	3.40×10^{12}	9020[4]
k_{td}	6.74×10^{10}	2533[4]
k_{fT}	3.92×10^8	4539[4]
k_{fM2}	2.12×10^{11}	9020[4]
k_{bb1}	6.55×10^{13}	8815
k_{bb2}	1.20×10^{14}	8298

On the other hand, the parameters tuned for fitting of the experimental results are listed in **Table 4**. There are two important considerations for this work with respect to literature. First, an additional chain transfer to monomer reaction (rate constant k_{fM2}), not considered in previous works,[4,18] is added to the kinetic scheme. Second, even though one single back-biting rate constant has been used in previous literature,[18] two separate back-biting reactions (and then the two corresponding rate constants) are used in this model to predict the experimental CF_2H and CH_3 end-group concentration with accuracy. It is worth noting that, in this work the effect of having head-to-tail addition is taken into account by the use of corresponding probability term, p_{HT}, (as shown in Section 2.4). This was not considered in the literature, therefore while comparing the values of the back-biting rate constants, one should multiply the value reported in the literature by the probability of having a tail type radical from a head type.

The activation energies reported in Table 4 are mostly taken from the literature[4] for the polymerization of the same monomer. The referred work uses a single value of activation energy for propagation and chain transfer to polymer and to chain-transfer agent due to the similarities of these reactions. Since the propagation to TDB is not considered in that work, we assume that the activation energy of the propagation to TDB is equal to that of chain transfer to polymer, due to similarity of the reactions. Another assumption is made for the activation energy of the bimolecular termination reaction: even though the referred work considers terminations occur only by combination, we used this same value for the bimolecular termination occurring by disproportionation considered in the model (due to experimental evidence mentioned in Section 2.1). Finally, the activation energy

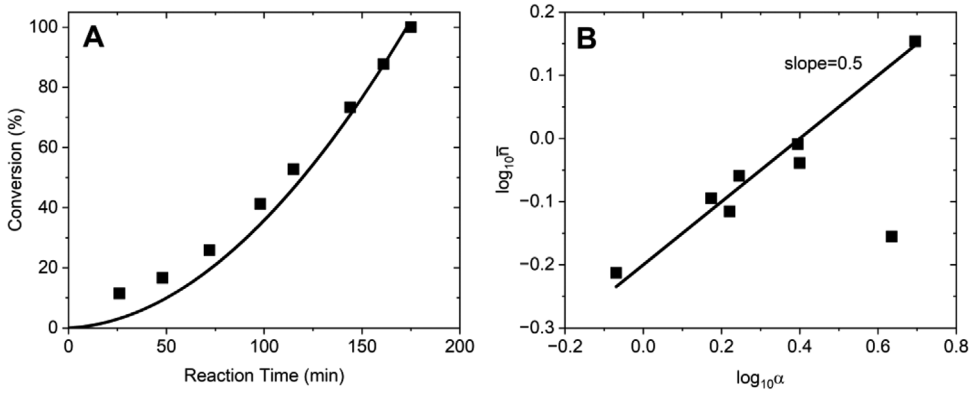

Figure 1. A) Conversion versus Time. Solid line: Model prediction. Squares: Experimental data. B) Plot of logarithm of average number of active chains per particle versus logarithm of rate of entry to termination. Solid line: straight line with slope 0.5. Squares: Experimental data.

Table 5. Values of Kinetic Parameters at 40, 90 °C, and the Literature Values.

Parameter	Value at 40 °C	Value at 90 °C	Literature Value [18]	Unit
k_{pM}	3.05×10^4	2.25×10^5	1.26×10^5	$L\ mol^{-1}\ min^{-1}$
k_{TDB}	3.28×10^2	2.42×10^3	1.17×10^3	$L\ mol^{-1}\ min^{-1}$
k_{fP}	7.96×10^{-1}	5.86×10^0	3.53×10^0	$L\ mol^{-1}\ min^{-1}$
k_{fM}	1.04×10^0	5.50×10^1	8.19×10^1	$L\ mol^{-1}\ min^{-1}$
k_{td}	2.06×10^7	6.28×10^7	3.24×10^6	$L\ mol^{-1}\ min^{-1}$
k_{fT}	1.97×10^2	1.45×10^3	1.39×10^3	$L\ mol^{-1}\ min^{-1}$
k_{fM2}	6.47×10^{-2}	3.43×10^0	Not available	$L\ mol^{-1}\ min^{-1}$
k_{bb1}	3.85×10^1	1.86×10^3	1.64×10^2	min^{-1}
k_{bb2}	3.68×10^2	1.42×10^4	1.64×10^2	min^{-1}

values for the back-biting reactions, not accounted for in the work of Pladis et al.[4] as two separate reactions, have been determined by fitting the chain-ends data at different reaction temperatures (according to results to be shown in Section 3.5).

Starting from the literature values as first guess, the model parameters have been estimated by fitting the model predictions to the experimental data. Such fitting was carried out solving the corresponding optimization problem by the genetic algorithm function available in MATLAB. Based on the results of the optimization and the activation energy values reported in Table 4, a set of pre-exponential factors are calculated in this work and are reported in the same table.

To make a comparison and assess the reliability of the estimated rate constants, a similar system close to the reaction conditions presented in this work is selected. [18] Using the optimized value of the initiator efficiency (f) of 8% and the set of parameters reported in Table 4, the rate constants are estimated at the lower and the upper temperatures (40 and 90 °C) of the literature work[18] and are reported in **Table 5**.

By looking at Table 5, one can see the agreement of the estimated rate constant with respect to the values reported in the literature. All of the rate constants reported in the literature lie within the range of values predicted at 40 and 90 °C using the pre-exponential factors estimated in this work, with the exception of bimolecular termination, chain transfer to monomer, and one of the back-biting rate constants (k_{bb2}), which remains anyhow still comparable. Given the general lack of experimental data for the system under consideration, such an overall agreement is considered good enough.

From this set of parameter values, the model results in terms of conversion during time are compared with experimental data in **Figure 1**A. The accelerating increase in the amount of polymer formed, typical for pseudo-bulk conditions, can be appreciated from both experimental and model results.

Given the relevance of the assumption of pseudo-bulk system, its actual applicability has been validated by experimental data of polymerization rate and particle size. The average number of radicals per particle $\bar{n}$ is calculated by Equation (26):

$$\bar{n} = \frac{\frac{dM_c}{dt}}{k_{pM}\ H\ P\ y}\ \frac{N_A V_w}{N_P} \tag{26}$$

where $\frac{dM_c}{dt}$ represents the rate of polymerized monomer, k_{pM} is the propagation rate constant, H is the Henry constant, P is the absolute pressure, y is used for the molar fraction of the monomer in the gas phase, N_A is the Avogadro's number, V_W is used to represent the volume of water and N_P is the number of particles. Then, the classical Smith-Ewart diagram[33] is obtained by plotting $\log_{10}\bar{n}$ against the ratio of radical entry to termination (parameter α) calculated by Equation (27). In that equation, f is used for the efficiency of the decomposition of the initiator, and k_d represents the rate constant for the decomposition of the initiator, N_I is the number of moles of initiator, v_p is the volume of a single particle and k_{td} is the termination by disproportionation rate constant.

$$\alpha = \frac{4 f k_d N_I N_A^2}{k_{td} N_P}\ v_p \tag{27}$$

The resulting plot is shown in Figure 1B: with the exception of one single experimental value (which has been assumed to be an outlier), all the data show good agreement with respect to a straight line with slope of 0.5. This evidence and also the fact that all the $\bar{n}$ values are above 0.5, as reported in Table S2 (Supporting Information), legitimate the adoption of the pseudo-bulk

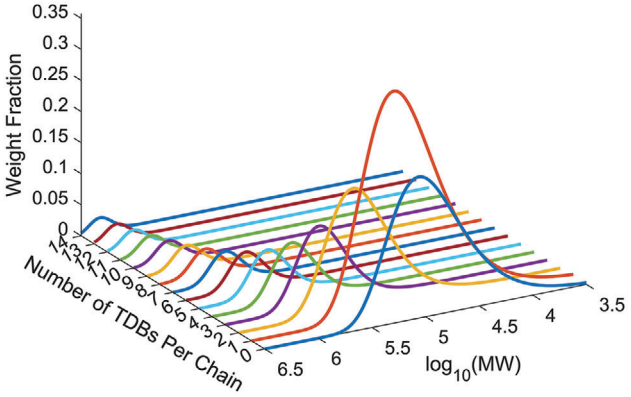

Figure 2. MWD of each polymer chain class.

assumption in model development,[33] which means that the particle number is not playing any role on the rate of polymerization. In fact, the large number of radicals per particle makes the system act as if it would be bulk polymerization.

3.2. Molecular Weight Distributions

Experimental molecular weight distributions are obtained by GPC. As already mentioned in Section 3.1, the used solvent can dissolve ≈92% of the total polymer, being the insoluble fraction filtered out. In order to have a fair comparison with experimental data, we removed the same mass fraction from the predicted distributions. To make clear the effect of removing the insoluble polymer fraction on the MWD, a figure comparing the results of the model without such removal (total polymer amount) and soluble polymer only is reported in Figure S2 (Supporting Information). Since more branched macromolecules are the most likely to form the insoluble fraction, the soluble part of the polymer was evaluated by accumulating the mass of produced polymer starting from the first class until 92% w/w of the produced polymer is collected, corresponding to the first 15 classes. Given the number of soluble classes, only the molecular weight distributions of those classes have been compared with the results of the GPC measurements. Accordingly, the predicted MWD of the polymer is obtained by summing the MWDs of each class for the soluble part. The MWDs of each class are reported in **Figure 2**.

It can be observed that most of the produced polymer belongs to class 1, hence having 1 TDB per chain. This is followed by class 0 where no TDB is present. From class 2 on, the intensity of the different distributions becomes smaller as the number of classes increases. Another observation is that the peaks shift to larger molecular weight as the number of classes increases, as expected for highly branched chains exhibiting larger numbers of TDBs.

The comparison of the MWD at different conversions (the area of each curve is proportional to the corresponding amount of produced polymer) stacked on top of each other are reported in **Figure 3** (derivation of the formula used to obtain weight fraction versus $\log_{10}$(MW) is reported in Equation S3 (Supporting Information). In all the cases, the model successfully predicted the location of the main peak, but also it successfully predicted the formation of a shoulder at large molecular weight. The only discrepancy between the predictions and the experiment comes from the magnitude of the shoulder at large conversion, which is slightly underestimated by the model. Given the limited accuracy of the experimental technique (≈ ±15%), this agreement was considered good enough. One important note to mention is that, as reported in Section 5, polystyrene (PS) standards have been used for GPC calibration. In order to make a fair comparison, the raw experimental data is corrected for PVDF using the Universal Calibration concept[34–36] along with literature values of the Mark-Houwink parameters for PS and PVDF in the specific solvent used for GPC analysis (dimethyl acetamide, DMAc).[37] These parameter values and the derivation of the correction factor are reported in Table S3 and Equation S4 (Supporting Information), respectively.

From the simulated MWDs, the number- and weight-average molecular weight are calculated and compared to the experimental results. According to **Figure 4**, both number and weight average molecular weight values are well predicted by the model, with some underestimation in the case of the first quantity (number average molecular weight). Given the well-known stronger reliability of GPC in terms of weight-average quantities, this agreement was also considered good enough.

3.3. Chain-Ends

Due to the head-tail nature of the monomer, two main chain-ends can be identified, namely CF_2H and CH_3. Both chain-ends are formed by the reactions that are producing a dead chain according to the kinetic scheme in Table 1. Specifically, those reactions are: i) chain transfer to polymer, ii) termination, and iii) chain transfer to CTA. Besides these reactions, back-biting reactions also produce a short branch, hence they also contribute to the production of chain-ends. Unlike the CF_2H type chain-end, the CH_3 type chain-end can also be produced by the propagation reactions of the initiator fragment. The balances for both chain-ends are reported in Equations (16) and (17), and the comparison with experimental NMR data are shown in **Figure 5**A,B, respectively.

As can be seen, the experimental data are quite constant during the reaction. According to the model equations and the used parameters, this behavior is expected and nicely predicted by the model. Moreover, the main reactions affecting the number of chain-ends of both types are the back-biting reactions, further supporting the need of having separate rate constants for each type of chain-end to accurately predict the experimental data.

3.4. Long Branches

Even though there is no experimental data on branches and TDBs, the model predicts such quantities. This information is used to check the self-consistency of the model: since TDBs can be formed at the end of a branch, the maximum number of TDBs is limited by the number of branches plus two (those of the backbone), in other words the relation TDB ≤ LCB + 2 has to be fulfilled. According to the kinetic scheme in Table 1, the branching points, that is, the molecular locations from which the long chain branches (LCBs) can grow, are produced by transfer to polymer and propagation to terminal double bond reaction. The model results are reported in **Figure 6**. By looking at the results, during

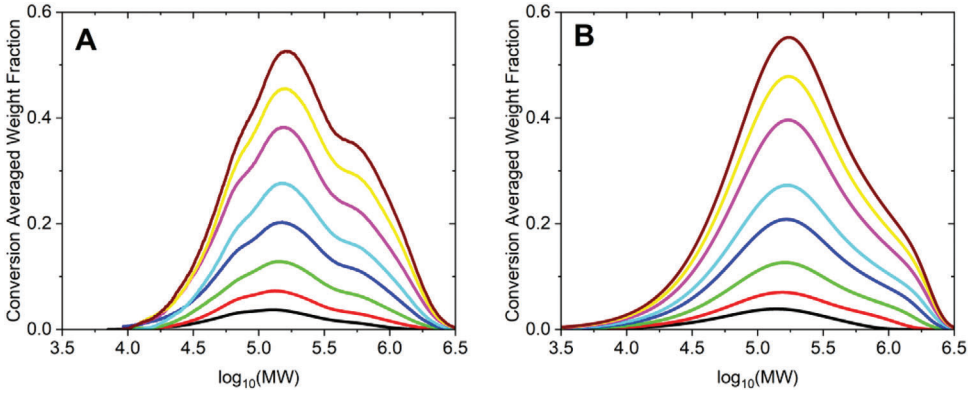

Figure 3. Conversion corrected stack of MWDs for (A) experimental data and (B) model predictions at different conversions. Black: 11%. Red: 17%. Green: 26%. Dark blue: 41%. Light blue: 53%. Purple: 73%. Yellow: 88%. Brown: 100%.

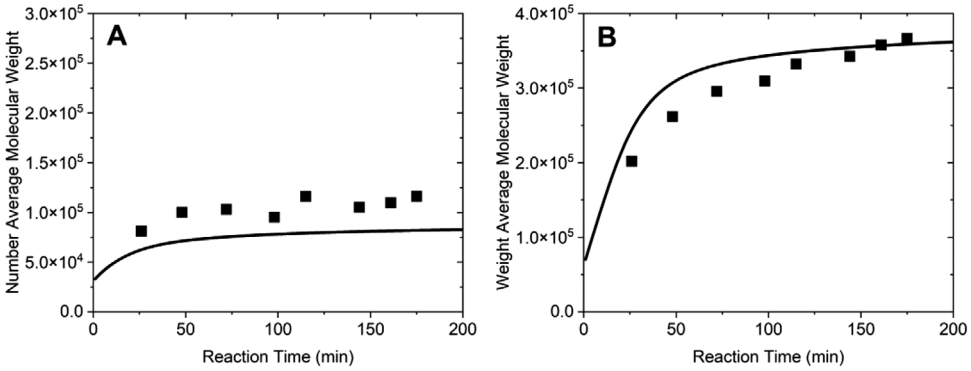

Figure 4. A) Number and B) weight average molecular weight. Solid lines: Model predictions. Squares: Experimental data.

the initial stage, the average number of TDBs is larger than that of LCBs, meaning mostly linear chains bearing some TDBs are formed. One important thing to mention is that the constraint between the moles of TDB and LCB discussed above is not violated since the difference between moles of LCB and TDB is not larger than 2. After the initial stage, the moles of LCB gets relatively closer to the moles of TDB until the end of the operation, which guarantees that the constraint is fulfilled throughout the reaction.

As already mentioned, the main advantage of the model reported herein is that the properties that define the classes (in our case the number of TDBs per chain) can be tracked as a function of the chain length, thus resulting in a 2D distribution of the microstructural properties, chain length and number of terminal double bonds. Such detail is lost using a conventional 1D model which would provide one single average value representative of the entire population of macromolecules. The distribution of TDBs, $TDB(n)$, with respect to the molecular weight is shown

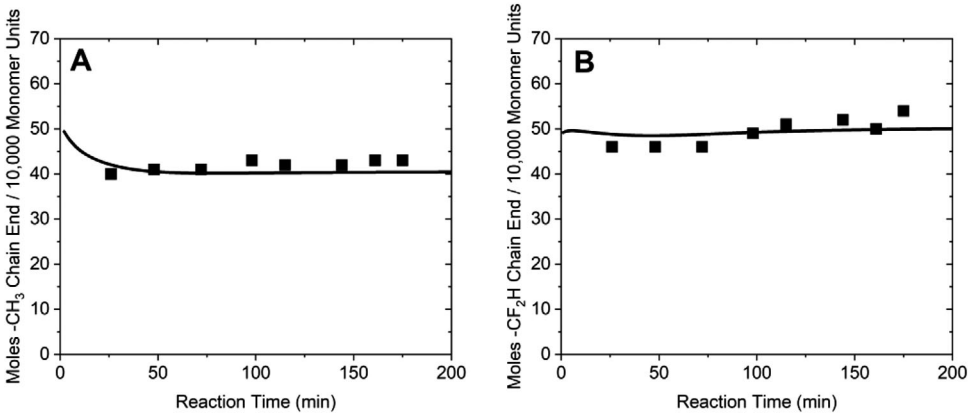

Figure 5. A) CH_3 chain-end. B) CF_2H chain-end. Solid line: Model predictions. Squares: Experimental data.

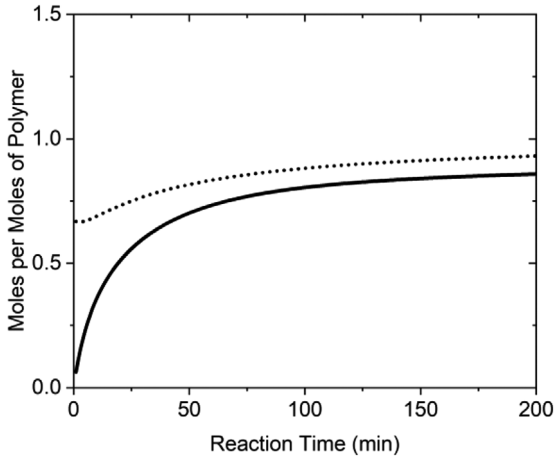

Figure 6. Comparison of LCB and TDB. Solid line: Long-chain branches. Dotted line: Terminal double bonds.

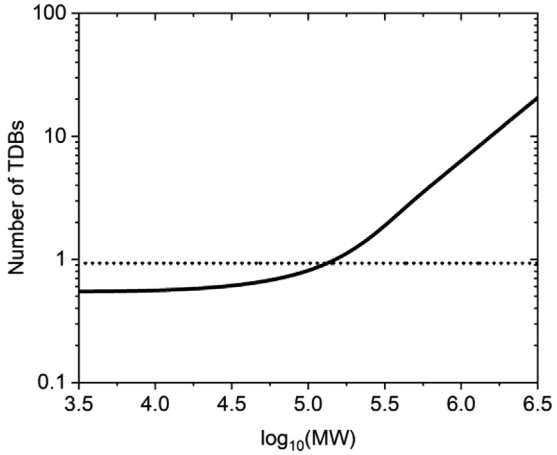

Figure 7. Distribution of TDBs as a function of molecular weight (solid line). Dotted line: population-average value.

in **Figure 7**, compared with the corresponding number-average value, TDB_n. The expressions used to calculate the distribution of TDBs and the average value are reported in Equations (28) and (29), respectively. In the equations, t is used to represent the number of TDBs, $f(n, t)$ is the distribution for a given chain length and number of TDBs as calculated by Equation (15), and TDB is used for the total moles of TDBs (calculated by Equation (23)) and μ_0 represents the total moles of produced polymer.

$$TDB(n) = \frac{\sum_{t=0}^{\infty} \left(tf(n,t)\right)}{\sum_{t=0}^{\infty} f(n,t)} \tag{28}$$

$$TD\,B_n = \frac{TDB}{\mu_0} \tag{29}$$

Using a single average value for the distribution, in this case 0.93, one would lose an important information, as a broad distribution of TDBs is obtained in this system, influencing the behavior of the polymer. According to the calculations, the short chains bear no (or very small number of TDBs), by far less than one per chain. However, as the chain gets larger, the number of TDBs per chain starts to steeply increase, which is expected since larger chains would have much larger probability to undergo branching reactions as well as reactions that produce TDBs. Long chains exhibit high heterogeneity, as it can be seen from the very high slope of the curve in Figure 7.

Table 6. Experimental Conditions of Experiments used for Model Validation.

	T/T_{ref} [-]	DTBP [mL/kg monomer]
Run 1	0.96	11.93
Run 2	0.97	11.65
Run 3	1.00	10.13
Run 4	1.00	10.66
Run 5	1.03	9.25
Run 6	1.03	9.25
Run 7	1.04	8.59

3.5. Model Validation

In order to check the reliability of the model predictions, an additional set of experiments using the same recipe of the reference reaction used for parameter evaluation (Run 3) and different temperatures and initiator amounts has been conducted, as summarized in **Table 6**. Note that the values in the table are expressed as ratio with respect to the reference experiment for confidentiality constraint.

Differently from the reference case, only final values of conversion and polymer properties (end groups and molecular weights) are available in this case, corresponding to a conversion of 100% Therefore, the comparison with the model prediction is carried out as a function of temperature (more precisely, with respect to the ratio of the reaction temperature to the reference temperature). In addition, it is assumed that the difference of DTBP amount in Run 3 (reference) and Run 4 is small enough, so they could be considered as identical runs.

In **Figure 8A**, the time required to reach the final conversion at the different reaction conditions is reported. Even though some discrepancy between experiments and model is present, the expected trend of decreasing reaction time at larger temperatures is well predicted. Given the usual irreproducibility of the time behavior of radical polymerization reactions at the industrial scale, such an agreement is believed to be good enough.

On the other hand, the model predictions are definitely good in terms of chain-ends, as shown in Figure 8B,C. This agreement is especially welcome given the impact of the temperature variation on the entire set of polymerization reactions.

Finally, the comparison in terms of number and weight average molecular weight is reported in Figure 8D,E. Just like the reference case reported in Figure 4, the model underestimates the number average molecular weight and is able to predict the weight average molecular weight nicely at different reaction conditions. Once more, this agreement is convincingly supporting model reliability and its prediction power with respect to relevant reaction parameters such as temperature and initiator amount.

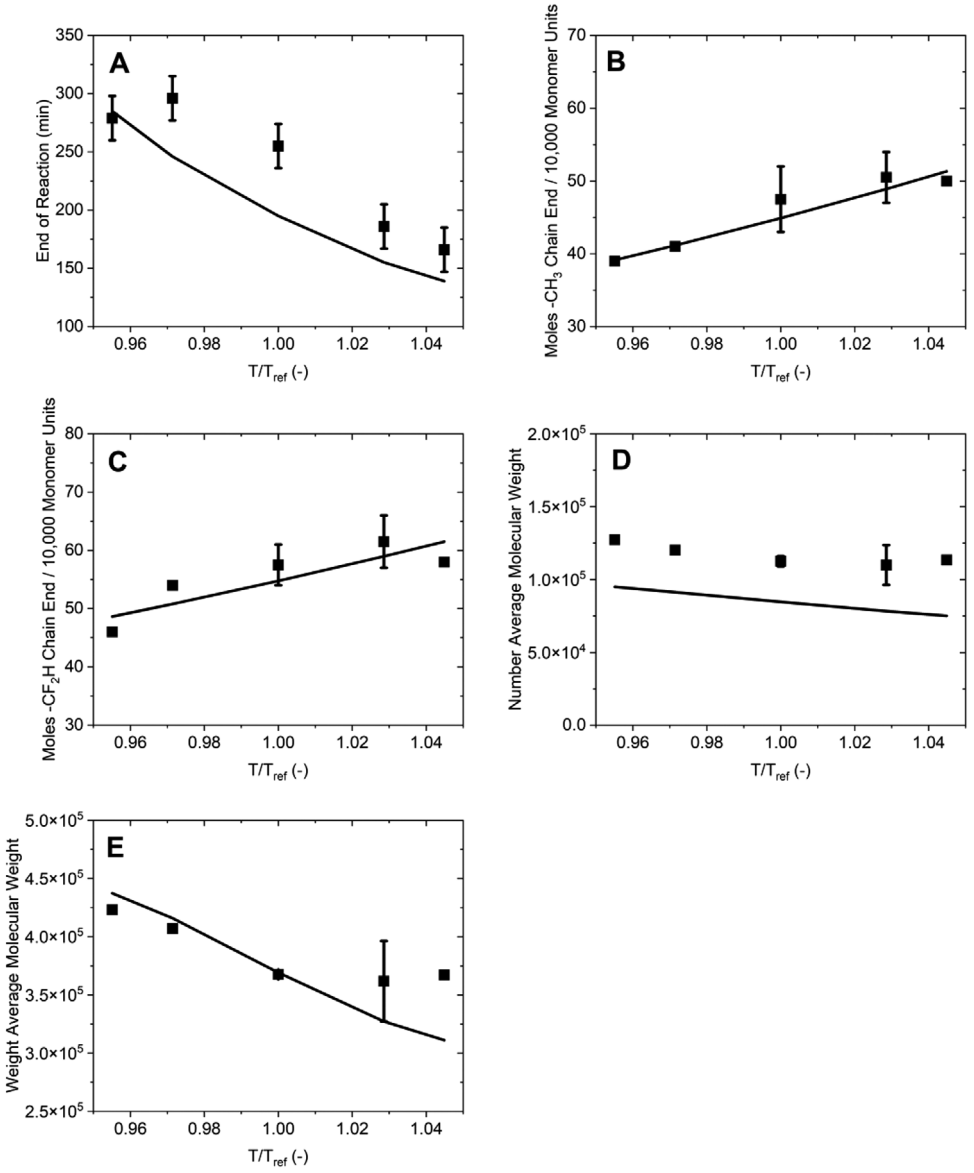

Figure 8. A) End of reaction at different reaction conditions. B) CH_3 and C) CF_2H chain-ends at different reaction conditions. D) Number and E) weight average molecular weight. Solid lines: Model predictions. Squares: Experimental data.

4. Conclusion

In this work, kinetic investigation of the emulsion polymerization of VDF is investigated. A reliable kinetic scheme with a set of reactions that are expected to take place in the system, and the kinetic constants for each of these reactions are presented. A 2D model, keeping track of the chain length as well as the number of terminal double bonds per chain is developed. Numerical solution of the model is achieved by method of moments, and the predictions are compared with experimental data.

In order to estimate reliable kinetic constants, a parameter optimization (using genetic algorithm) is carried out. The optimized parameters showed good agreement with the kinetic constants reported in the literature for similar systems, as well as the model predictions when comparison for the amount of produced polymer, main chain-ends, number and weight average molecular weights as well as molecular weight distributions for different amounts of produced polymer are carried out. The good agreement of the model predictions is achieved not only for a reference reaction, but also for a set of validation experiments which are carried out at different temperatures and different initiator amounts.

One of the main values of this work is the prediction of the TDB distribution, which shows the heterogeneity of the system. This precise prediction is useful especially when the final application is considered. Using the 2D model mentioned in this work, we were able to predict full MWD nicely. It is worth mentioning that this approach can be further deepened. In other words, in

case more precise predictions are needed, for example, if the distribution for the branching points is required, one can increase the dimension of the model.

5. Experimental Section

Experimental Setup: The polymerization reactions are carried out using a stainless-steel reactor. The temperature was kept constant at the desired value using an external jacket. The reactor is first filled with 3.1 L of water per unit mass (1 kg) of monomer, then the system is heated to the reaction temperature and vented. The desired pressure is reached by feeding the gaseous VDF in the system. Once the pressure is stable at the target value, 14.3 mL of di-tert-butyl peroxide (DTBP), used as initiator, per unit mass of monomer are fed into the reactor as a single shot. The ignition time is estimated as the one corresponding to a pressure decrease of 0.1 bar below the target value. Then, the monomer feed is started in order to keep the pressure constant and the reaction is run until the desired amount of VDF has been injected. At this point, the reactor is cooled down at room temperature, the system is slowly vented and the latex is recovered.

Characterization of the Polymer: The MWD of the produced polymer is measured by gel permeation chromatography (GPC). The analysis is performed using dimethyl acetamide (DMAc) using the following details:

Columns: Styragel HT6, HT5, HT4, HT3, Styragel DMF Guard Column 4.6 × 30 mm St; Test Temperature: 45 °C; Calibration standards: polystyrene standards having MW between 1700 and 4000,000 Da; Injected volume: 100 µl; Flow rate: 1 ml min^{-1}; Detector: Refractive index detector; Evaluation of the insoluble polymer fraction: Centrifugation at 20000 RPM for 1 h at 10 °C and drying at 150 °C for 48 h.

The chain-ends are measured by nuclear magnetic resonance spectroscopy (NMR) performed on an Agilent DirectDrive System 500 operating at 499.86 MHz for ^{1}H and 470.29 MHz for ^{19}F NMR. The polymer is dissolved in deuterated acetone. ^{1}H and ^{19}F NMR spectra are used for analyzing the concentration of the chain-ends per 10000 monomer units.

Supporting Information

Supporting Information is available from the Wiley Online Library or from the author.

Acknowledgements

Open access publishing facilitated by Politecnico di Milano, as part of the Wiley - CRUI-CARE agreement.

Conflict of Interest

The authors declare no conflict of interest.

Data Availability Statement

The data that support the findings of this study are available from the corresponding author upon reasonable request.

Keywords

emulsion polymerization, kinetic model, method of classes, polymer microstructure, vinylidene fluoride

Received: July 19, 2024
Revised: September 25, 2024
Published online:

[1] B. Ameduri, *Chem. Rev.* **2009**, *109*, 6632.
[2] J. E. Marshall, A. Zhenova, S. Roberts, T. Petchey, P. Zhu, C. E. J. Dancer, C. R. McElroy, E. Kendrick, V. Goodship, *Polymers (Basel)* **2021**, *13*, 1354.
[3] R. Siegmann, M. Drache, S. Beuermann, *J. Fluor. Chem.* **2014**, *159*, 48.
[4] P. Pladis, A. H. Alexopoulos, C. Kiparissides, *Ind. Eng. Chem. Res.* **2014**, *53*, 7352.
[5] S. Beuermann, M. Imran-ul-haq, *Macromol. Symp.* **2007**, *259*, 210.
[6] Y. Patil, J. Zhao, B. Ameduri, S. Rastogi, *Macromolecules* **2024**, *57*, 616.
[7] R. Siegmann, E. Möller, S. Beuermann, *Macromol. Rapid Commun.* **2012**, *33*, 1208.
[8] J. Schwaderer, M. Drache, S. Beuermann, *Molecules* **2024**, *29*, 1551.
[9] J. Guiot, B. Ameduri, B. Boutevin, *Macromolecules* **2002**, *35*, 8694.
[10] J. M. Asua, *Polymer Reaction Engineering*, Wiley, New York Chichester, UK **2007**.
[11] J. M. Asua, *J. Polym. Sci. Part A Polym. Chem.* **2004**, *42*, 1025.
[12] S. C. Thickett, R. G. Gilbert, *Polymer (Guildf)* **2007**, *48*, 6965.
[13] A. M. van Herk, *Chemistry and Technology of Emulsion Polymerisation*, Wiley, New York Chichester, UK **2013**.
[14] B. Brooks, *Chem. Eng. Technol.* **2010**, *33*, 1737.
[15] H. G. Yuan, G. Kalfas, W. H. Ray, *J. Macromol. Sci. Part C Polym. Rev.* **1991**, *31*, 215.
[16] E. Vivaldo-Lima, P. E. Wood, A. E. Hamielec, A. Penlidis, *Ind. Eng. Chem. Res.* **1997**, *36*, 939.
[17] M. Fuentes-Exposito, S. Norsic, T. Février, P.-Y. Dugas, S. Boutti, S. Devisme, A. Bonnet, F. D'Agosto, M. Lansalot, *Polym. Chem.* **2021**, *12*, 5640.
[18] M. Apostolo, V. Arcella, G. Storti, M. Morbidelli, *Macromolecules* **1999**, *32*, 989.
[19] G. Zapsas, Y. Patil, Y. Gnanou, B. Ameduri, N. Hadjichristidis, *Prog. Polym. Sci.* **2020**, *104*, 101231.
[20] K. N. Thakore, H. M. Mehendale, *Encycl. Toxicol. Third Ed.* **2014**, *2*, 149.
[21] M. Imran-ul-haq, B. Tiersch, S. Beuermann, *Macromolecules* **2008**, *41*, 7453.
[22] E. Mavroudakis, D. Cuccato, M. Dossi, G. Comino, D. Moscatelli, *J. Phys. Chem. A* **2013**, *118*, 238.
[23] C. Zander, K. D. Hungenberg, T. Schall, C. Schwede, U. Nieken, *Macromol. React. Eng.* **2020**, *14*, 2000009.
[24] E. Mastan, S. Zhu, *Eur. Polym. J.* **2015**, *68*, 139.
[25] M. Apostolo, V. Arcella, G. Storti, M. Morbidelli, *Macromolecules* **2002**, *35*, 6154.
[26] F. Teymour, J. D. Campbell, *Macromolecules* **1994**, *27*, 2460.
[27] Y. Yu, E. J. Fischer, G. Storti, M. Morbidelli, *Ind. Eng. Chem. Res.* **2014**, *53*, 7333.
[28] P. Pladis, C. Kiparissides, *Chem. Eng. Sci.* **1998**, *53*, 3315.
[29] G. Papavasiliou, F. Teymour, *Ind. Eng. Chem. Res.* **2005**, *44*, 2754.
[30] H. M. Hulburt, S. Katz, *Chem. Eng. Sci.* **1964**, *19*, 555.
[31] L. Batt, G. N. Robinson, *Int. J. Chem. Kinet.* **1987**, *19*, 391.
[32] H. J. Curran, *Int. J. Chem. Kinet.* **2006**, *38*, 250.
[33] J. Ugelstad, P. C. Mörk, J. O. Aasen, *J. Polym. Sci. Part A-1 Polym. Chem.* **1967**, *5*, 2281.
[34] J. V. Dawkins, *Eur. Polym. J.* **1977**, *13*, 837.
[35] G. Glöckner, *Polymer Characterization by Liquid Chromatography*, Elsevier, Amsterdam / New York **1987**.
[36] P. C. Painter, M. M. Coleman, *Essentials of Polymer Science and Engineering*, DEStech Publ. Inc., Lancaster USA **2008**.
[37] G. Welch, *Polymer (Guildf)* **1974**, *15*, 429.

